Angular Dependence of Internal Energy Distributions of Activated $Fe(CO)_5^{\cdot+}$ and $W(CO)_6^{\cdot+}$ Ions. The Contributions of Vibrational and Electronic Excitation Mechanisms in Kiloelectron Volt Collisions

S. R. Horning, M. Vincenti, and R. G. Cooks*

Contribution from the Department of Chemistry, Purdue University, West Lafayette, Indiana 47907, and Instituto Guido Donegani, S.p.A., 28100 Novara, Italy.
Received July 25, 1988

Abstract: The average internal energy deposited into $Fe(CO)_5^{\cdot+}$ and $W(CO)_6^{\cdot+}$ upon kiloelectron volt collision-induced dissociation (CID) using Ar as a target gas increases with both the collision energy (E) and the angle (θ) through which the collision products are collected. An average energy of 7–8 eV is deposited into the $Fe(CO)_5^{\cdot+}$ ion as it is scattered through a laboratory scattering angle of 2° in a 3-keV collision with Ar. Similar average internal energies are deposited into $W(CO)_6^{\cdot+}$ at corresponding laboratory scattering angles, the smaller center-of-mass collision energy E_{cm} for $W(CO)_6^{\cdot+}$ being compensated for by a larger value of θ_{cm}, making the scattering parameter, $(E\theta)_{cm}$, similar for both systems. Collision activation experiments performed with He and C_9F_{20} as target gases show that the effective mass of the latter is much less than its molecular weight, suggesting that the target is internally excited and/or that parts of the target are spectators during collisional activation. The distribution $P(\epsilon)$ of internal energies acquired upon collisional activation is dependent upon the collision energy, the scattering angle, and the nature of the collision gas. The distributions are typically Gaussian in shape at 1.5- and 2-keV collision energies for scattering angles in the range 1 to 2° for the title projectiles. In contrast, distributions for ions scattered through similar angles upon 3-keV collisions are distinctly bimodal in shape. The lower energy component in the bimodal distribution is thought to be due to electronic excitation, while the higher energy component is associated with a vibrational excitation mechanism, as suggested by comparison with energy distributions obtained for electron impact, low-energy (electron volt) collision-activation, and surface-induced dissociation (SID). An approximately linear relationship is found between the energy deposited and the reduced scattering parameter $E\theta$. These data confirm earlier suggestions that angle-resolved mass spectrometry (ARMS) can be used to select the degree of activation of a mass-selected ion. They also provide evidence that direct vibrational excitation is a significant activation mechanism in collisional activation of polyatomic ions in the keV energy range.

Angle-resolved mass spectrometry (ARMS) is an experiment in which product ions resulting from collision-induced dissociation (CID) are collected through selected laboratory scattering angles.[1-4] ARMS measurements are normally performed at high (kiloelectron volt) collision energies using modified, double-focusing mass spectrometers,[5-11] but low-energy (electron volt) angle-resolved experiments have also been conducted in specially constructed beam instruments.[12-14] Although several factors may contribute to product ion scattering, including isotropic release of kinetic energy during fragmentation,[4,15-19] increasing the scattering angle has been shown by qualitative studies on a variety of systems to allow selection of ions which undergo conversion of an increasing fraction of their translational energy into internal energy during the collision process.[4,8,9,15] Moreover, in experiments at low collision energies the scattering angle/internal energy relationship has been established definitively.[12a] Since the internal energy of an ion controls its fragmentation behavior, selection of internal energy is of practical importance in analytical applications of tandem mass spectrometry.[20] A number of persuasive examples are now available in which the ARMS technique has been used to examine fragmentation reactions and ion structures[21] and to select ion internal energies, although the association of degree of activation with scattering angle has not been universally accepted.[16,22]

The process of collision-induced dissociation (CID) has been investigated in detail, and many features of the mechanism for inelastic energy transfer, particularly the conversion of translational to internal energy during the collision process, have been established.[17,23-25] It is generally assumed that upon low-energy (<200-eV lab) collisions, excitation occurs through a vibrational transition within the ground electronic state of the ion,[12,14,26] and that dissociation follows excitation and occurs in accord with the tenets of the quasi-equilibrium theory.[27] An alternative excitation mechanism is found for high-energy (kiloelectron volt) collisions, where, for high-velocity, low-mass ions, vertical Franck–Condon transitions are known to be involved.[23-25] Upon activation, the excited ion rapidly redistributes its energy via an internal con-

* Address correspondence to this author at Purdue University.

(1) (a) Cooks, R. G.; Kim, K. C.; Beynon, J. H. *Chem. Phys. Lett.* **1973**, *23*, 190. (b) Ast, T.; Terwilliger, D. T.; Cooks, R. G.; Beynon, J. H. *J. Phys. Chem.* **1975**, *79*, 708. (c) Medved, M.; Cooks, R. G.; Beynon, J. H. *Chem. Phys.* **1976**, *15*, 295. (d) Laramee, J. A.; Carmody, J. J.; Cooks, R. G. *Int. J. Mass Spectrom. Ion Processes* **1979**, *31*, 333. (e) Kingston, E. E.; Brenton, A. G.; Boyd, R. K.; Beynon, J. H. *Int. J. Mass Spectrom. Ion Processes* **1983**, *47*, 117.

(2) Boyd, R. K.; Kingston, E. E.; Brenton, A. G.; Beynon, J. H. *Proc. R. Soc. London, A* **1984**, *392*, 59.

(3) Van der Zande, W. J.; De Bruijn, D. P.; Los, L.; Kistemaker, P. G.; McLuckey, S. A. *Int. J. Mass Spectrom. Ion Processes* **1985**, *67*, 161.

(4) Moore, C.; Mason, R. S.; Jennings, K. R.; Evans, S. *Int. J. Mass Spectrom. Ion Processes* **1988**, *86*, 109.

(5) Hemberger, P. H.; Laramee, J. A.; Hubik, A. R.; Cooks, R. G. *J. Phys. Chem.* **1981**, *85*, 2335.

(6) Hubik, A. R.; Hemberger, P. H.; Laramee, J. A.; Cooks. R. G. *J. Am. Chem. Soc.* **1980**, *102*, 3997.

(7) Laramee, J. A.; Hemberger, P. H.; Cooks, R. G. *Int. J. Mass Spectrom. Ion Processes* **1980**, *33*, 231.

(8) McLuckey, S. A.; Cooks, R. G. In *Tandem Mass Spectrometry*; McLafferty, F. W., Ed.; Wiley: New York, 1983; p 303.

(9) (a) Franchetti, V.; Carmody, J. J.; Krause, D. A.; Cooks, R. G. *Int. J. Mass Spectrom. Ion Processes* **1978**, *26*, 353. (b) Fedor, D. M.; Cooks, R. G. *Anal. Chem.* **1980**, *52*, 679. (c) Frison, G.; Cecchinato, F.; Traldi, P. *Rapid Comm. Mass. Spectrom.* **1988**, *2*, 268.

(10) (a) Mason, R. S.; Farncombe, M. J.; Jennings, K. R.; Cooks, R. G. *Int. J. Mass Spectrom. Ion Processes* **1982**, *43*, 327. (b) Verma, S.; Ciupek, J. D.; Cooks, R. G.; Schoen, A. E.; Dobberstein, P. *Int. J. Mass Spectrom. Ion Processes* **1983**, *52*, 311.

(11) Boyd, R. K.; Kingston, E. E.; Brenton, A. G.; Beynon, J. H. *Proc. R. Soc. London. A* **1984**, *392*, 89.

(12) (a) Herman, Z.; Futrell, J. H.; Friedrich, B. *Int. J. Mass Spectrom. Ion Processes* **1984**, *58*, 181. (b) Vestal, M. L.; Blakley, C. R.; Futrell, J. H. *Phys. Rev. A* **1978**, *17*, 1321.

(13) Hirst, D. M.; Jennings, K. R.; Laramee, J. A.; Shukla, A. K. *Int. J. Mass Spectrom. Ion Processes* **1985**, *64*, 335.

(14) Dawson, P. H. *Int. J. Mass Spectrom. Ion Processes* **1983**, *50*, 287.

(15) McLuckey, S. A.; Verma, S.; Cooks, R. G.; Farncombe, M. J.; Mason, R. S.; Jennings, K. R. *Int. J. Mass Spectrom. Ion Processes* **1983**, *48*, 423.

(16) Todd, P. J.; Warmack, R. J.; McBay, E. H. *Int. J. Mass Spectrom. Ion Processes* **1983**, *50*, 299.

0002-7863/90/1512-119$02.50/0

version process, yielding vibrationally excited ions in their ground electronic state.[17,23,28] These ions may then dissociate, again in a delayed statistically controlled process.[27] Electronic excitation occurs without momentum transfer and, as a result, leads to zero scattering of the projectile ion during the collision process.[17,23,25] In most conventional mass spectrometers any scattering which might accompany high-energy CID is not observed, since only ions falling within an angle of approximately 0.2° can reach the detector.[2,9,18]

Alternatives to electronic excitation in the keV range of energies have been proposed.[18,23,25,29] A mechanism based on polarization forces which leads to vibronic excitation has long been recognized.[30,31] However, it leads to little scattering and is generally considered to be of limited importance for polyatomic ions. More significantly, an impulsive collision has been invoked to account for direct vibrational excitation[32] by a process in which atoms, or groups of atoms within one or both collision partners, act as spectators,[17,23,33] while others are directly involved in the collision. Such a mechanism results in large angle scattering and may account for the changes in the degree of ion excitation with scattering angle which have been observed in previous ARMS experiments.[4,7,8,15,21] Evidence for vibrational excitation in keV collisions of small polyatomic ions has been obtained by McLuckey et al., who observed that acetone ions undergo scattering up to 0.8° as a result of a vibrational or vibronic excitation upon collisional activation with He atoms at 5-keV collision energy.[3,34] In addition, Derrick et al. performed trajectory calculations and provided other evidence which supports the occurrence of direct vibrational excitation during collisions of large multiatomic ions upon He at kiloelectron volt energies.[29] At this time, however, there is no direct experimental evidence supporting the occurrence of both electronic and vibrational activation mechanisms in a single system. Nor is there information on the internal energy distributions associated with vibrational excitation in the keV regime, nor is the dependence of this process on scattering angle or collision energy known.

The purpose of this study was to investigate the manner in which the distribution $P(\epsilon)$ of internal energies deposited in selected parent ions varies with the scattering angle in high-energy collisions. $Fe(CO)_5^{\cdot+}$ and $W(CO)_6^{\cdot+}$ were chosen as the most appropriate parent ions for this investigation, since they undergo predominantly a simple, well-established sequence of fragmentation reactions from which their internal energy distributions can be inferred.[35] Parameters considered in this work included the scattering angle (θ), the kinetic energy of the colliding ion (E), and also, to a limited extent, the pressure and nature of the target gas.[36] The results obtained in these experiments are important since they clearly establish the increase in average ion internal energy ($\bar{\epsilon}$) with both the scattering angle (θ) and translational energy (E) of the projectile ion. The internal energy distributions, $P(\epsilon)$, measured in the present study also provide new insights into the mechanism of activation in high-energy CID, including the occurrence of direct vibrational excitation and some information on how the energy deposition in this process varies with collision parameters. These data represent the first internal energy distributions for ARMS and experimental evidence that activation in nonzero angle, high-energy CID may occur with considerable contribution from a vibrational excitation mechanism.

Experimental Section

ARMS experiments were performed on two mass spectrometers, a Finnigan MAT HSQ-30[37,38] (BEQQ-hybrid instrument: B = magnetic sector, E = electric sector, Q = quadrupole) and a Finnigan MAT 8400 (BE) instrument.[38] Both mass spectrometers have identical ion sources and double-focusing BE analyzers. The 8400 is modified to incorporate a 20-keV postacceleration conversion dynode, rather than a 5-keV dynode, which is employed on the HSQ-30. The scattering angle was selected through electrical deflection of the ion beam in the nonfocusing z direction[39] upon leaving the ion source and prior to entering the collision cell in the first field-free region.[10] Product ions resulting from collision-induced dissociation are transmitted through the magnetic and electrostatic analyzers only when they are scattered through an angle identical with that through which they were deflected initially, so keeping them on a path parallel to the original beam, but displaced from it in the nonfocusing z direction.[40] The analyzer aperture has a height of 5 mm in the z direction and the intermediate β-slit a height of 10 mm. In the focusing y direction, the β-slit was set at its widest value (2 mm) to maximize signal. Laboratory scattering angles of up to 2.3°[41] were accessed without instrument modifications. Scattering angles were estimated by calculating electrostatic deflection due to parallel plate z electrodes, and these values were corroborated using the SIMION ion optical program.[42] Angle-resolved data for methanol and n-butylbenzene

(17) Singh, S.; Harris, F. W.; Boyd, R. K.; Beynon, J. H. *Int. J. Mass Spectrom. Ion Processes* **1985**, *66*, 131.
(18) Singh, S.; Harris, F. W.; Boyd, R. K.; Beynon, J. H. *Int. J. Mass Spectrom. Ion Processes* **1985**, *66*, 151.
(19) Singh, S.; Thacker, M. S.; Harris, F. W.; Beynon, J. H. *Org. Mass Spectrom.* **1985**, *20*, 156.
(20) (a) Baer, T. In *Gas Phase Ion Chemistry*; Bowers, M. T., Ed.; Academic Press: New York, 1979; Vol. 1, p 153. (b) Baer, T.; Werner, A. S.; Tsai, B. P.; Lin, S. F. *J. Chem. Phys.* **1974**, *61*, 5468.
(21) (a) Fedor, D. M.; Cody, R. B.; Burinsky, D. J.; Freiser, B. S.; Cooks, R. G. *Int. J. Mass Spectrom. Ion Processes* **1981**, *39*, 55. (b) Burinsky, D. J.; Glish, G. L.; Cooks, R. G.; Zwinselman, J. J.; Nibbering, N. M. M. *J. Am. Chem. Soc.* **1981**, *103*, 465. (c) Verma, S.; Ciupek, J. D.; Cooks, R. G. *Int. J. Mass Spectrom. Ion Processes* **1984**, *62*, 219. (d) Zwinselman, J. J.; Nacson, S.; Harrison, A. G. *Int. J. Mass Spectrom. Ion Processes* **1985**, *67*, 93. (e) Reid, C. J.; Harris, F. M. *Int. J. Mass Spectrom. Ion Processes* **1988**, *85*, 151. (f) Vincenti, M.; Horning, S. R.; Cooks, R. G. *Org. Mass Spectrom.* **1988**, *23*, 585. (g) Wysocki, V. H.; Ross, M. M.; Horning, S. R.; Cooks, R. G. *Rapid Comm. Mass Spectrom.* **1988**, *2*, 214. (h) Brodbelt-Lustig, J. S.; Cooks, R. G. *Int. J. Mass Spectrom. Ion Processes* **1988**, *86*, 253. (i) Cooks, R. G.; Mabud, Md. A.; Horning, S. R.; Jiang, X.-Y.; Paradisi, C.; Traldi, P. *J. Am. Chem. Soc.* **1989**, *111*, 859.
(22) Waddell, D. S.; Boyd, R. K.; Brenton, A. G.; Beynon, J. H. *Int. J. Mass Spectrom. Ion Processes* **1986**, *68*, 71.
(23) Durup, J. In *Recent Developments in Mass Spectrometry*; Ogata, K., Hayakawa, T., Eds.; University of Tokyo Press: Tokyo, 1970, p 921.
(24) Cooks, R. G., Ed. In *Collision Spectroscopy*; Plenum Press: New York, 1978.
(25) Busch, K. L.; Glish, G. L.; McLuckey, S. A. In *Mass Spectrometry/Mass Spectrometry: Techniques and Applications of Tandem Mass Spectrometry*; VCH Publishers: New York, 1988; Chapter 3.
(26) Dawson, P. H.; Douglas, P. J. In *Tandem Mass Spectrometry*; McLafferty, F. W., Ed.; Wiley: New York, 1983; p 125.
(27) (a) Levson, K. In *Fundamental Aspects of Organic Mass Spectrometry*; Verlag Chemie: New York, 1978. (b) Robinson, P. J.; Holbrook, K. A. In *Unimolecular Reactions*; Wiley: New York, 1972.
(28) (a) Todd, J. P.; McLafferty, F. W. In *Tandem Mass Spectrometry*; McLafferty, F. W., Ed.; Wiley: New York, 1983; p 149. (b) Levson, K.; Schwartz, H. *Mass Spectrom. Rev.* **1983**, *2*, 77.
(29) (a) Gilbert, R. G.; Sheil, M. M.; Derrick, P. J. *Org. Mass Spectrom.* **1985**, *20*, 430. (b) Neumann, G. M.; Derrick, P. J. *Org. Mass Spectrom.* **1984**, *19*, 165.
(30) Los, J.; Govers, T. R. In *Collision Spectroscopy*; Cooks, R. G., Ed.; Plenum Press: New York. 1978; Chapter 6.
(31) Russek, A. *Physica* **1970**, *48*, 165.
(32) (a) Mahan, B. H. *J. Chem. Phys.* **1970**, *52*, 5221. (b) Uggerud, E.; Derrick, P. J. *Z. Naturforsch.* **1989**, *44a*, 245.
(33) (a) Fernandez. S. M.; Eriksen, F. J.; Bray, A. V.; Pollack, E. *Phys. Rev. A* **1975**, *12*, 1252. (b) Andersen, N.; Vedder, M.; Russek, A.; Pollack, E. *Phys. Rev. A* **1980**, *21*, 782. Compare: Henglein, A.; Muccini, G. A. *Z. Naturforsch.* **1962**. *17a*, 452.
(34) Van der Zande, W. J.; McLuckey, S. A.; De Bruijn, D. P.; Los, L.; Kistemaker, P. G. In *Proceedings of the 10th International Mass Spectrometry Conference, Swansea*; Todd, J. F. J., Ed.; Wiley: London, 1986; p 1123.
(35) (a) Wysocki, V. H.; Kenttämaa, H. I.; Cooks, R. G. *Int. J. Mass Spectrom. Ion Processes* **1987**, *75*, 181. (b) Kenttämaa, H. I.; Cooks, R. G. *Int. J. Mass Spectrom. Ion Processes* **1985**, *64*, 79.
(36) Laramee, J. A.; Cameron, D.; Cooks, R. G. *J. Am. Chem. Soc.* **1981**, *103*, 12.
(37) Schoen, A. E.; Amy, J. W.; Ciupek, J. D.; Cooks, R. G.; Dobberstein, P.; Jung, G. *Int. J. Mass Spectrom. Ion Processes* **1985**, *65*, 125.
(38) Finnigan MAT GmbH, Postfach 14 40 62, D-2800, Bremen, FRG.
(39) On the HSQ-30 and 8400 mass spectrometers the nonfocusing direction is labeled as the y direction and ARMS experiments are performed by applying asymmetric voltages across the y plates. We have chosen, however, to use earlier established nomenclature and refer to the nonfocusing direction as the z direction, rather than the y direction (see, for example, ref 1, 9, 10).
(40) The range of scattering angles accepted at 0° is ca. ±0.2°, viz, 0.4° in the xz plane and perhaps more in the focusing xy plane.
(41) The largest scattering angle was limited by the maximum voltage difference which could be applied between the z axis deflection plates (ca. 330 V).
(42) Written by J. A. Morrison and D. McGilvery; modified and made available by: Dahl, D. A.; Delmore, J. E. MS 2208, EE&G Idaho Inc., Idaho National Engineering Laboratory, P.O. Box 1625, Idaho Falls, ID 83415.

molecular ions obtained using this method of electrical deflection matched qualitatively with data obtained in earlier studies, where angle resolving slits were used to mechanically select the scattering angle.[7,15]

$Fe(CO)_5$ and $W(CO)_6$ were introduced into an unheated ion source through a sample leak inlet and ionized by 70-eV EI. Daughter ions generated upon CID of the molecular ion using selected target gases (He, Ar, and perfluoro-2,4-dimethyl-3-ethylpentane (C_9F_{20})) in the first field-free region collision cell were recorded via a B/E-linked scan of the sector analyzers.[43] A range of sample ($8 \times 10^{-8} - 4 \times 10^{-6}$ Torr) and Ar collision gas pressures (nominally 8×10^{-7}–3×10^{-5} Torr,[44] corresponding to attenuation of the parent ion signal by less than 2% to more than 50%) were utilized so that scattering effects due to possible multiple collisions could be detected. Under conditions where no collision gas was introduced, a low abundance of $(M - CO)^{\bullet+}$ fragment ion could be observed owing to metastable decomposition of the molecular ion. No other daughter ions were observed. As the collision gas pressure was raised to cause increasing main beam attenuation, no significant changes in the relative abundances of ions in the ARMS spectra at any scattering angle were noted, although there was an increase in the overall fragment ion abundance. For collisions upon He and C_9F_{20}, target gas was added until the parent signal was attenuated by 20%, yielding nominal pressures of 2×10^{-5} and 1×10^{-5} Torr, respectively. Mass-dependent discrimination effects, which may lead to errors in the data,[10] were evaluated by performing the B/E-linked scans at several different ratios of electrostatic analyzer to acceleration voltages. The relative abundances of low- to high-mass fragment ions in the daughter spectra varied by less than 10% at the maximum and minimum voltages in which fragment ions pass through the electrostatic analyzer, even at the largest scattering angles. Subsequently, for $Fe(CO)_5^{\bullet+}$ molecular ions, the analyzer voltage was selected by maximizing the high- and low-mass daughter ion signals at a scattering angle of 1.5°. $W(CO)_6^{\bullet+}$ was examined in a similar manner. In addition, the known relative abundances of the tungsten isotopes were used to finely adjust the electrostatic analyzer voltage in the B/E-linked scan analysis. Mass-dependent effects associated with discrimination in the detector are judged negligible, given the good agreement between the two instruments which operate at very different detector voltages.

Kinetic energy release measurements for dissociation of the activated $Fe(CO)_5^{\bullet+}$ ion, as well as for $Fe(CO)_4^{\bullet+}$ and $Fe(CO)_3^{\bullet+}$, were made using a custom-built MIKES instrument.[45,46] Kinetic energy release (T) values and the corresponding maximum scattering angles resulting from the excess energy released into translation were calculated from the ion kinetic energy peak widths (fwhm) corrected for the width of the main beam.[16,47] The undissociated primary ion beam encompassed a range of kinetic energies of less than 0.22 eV, corresponding to an energy resolution of 1100, and its total angular spread was estimated to be 0.37° in the xz plane.[36] The kinetic energy release values (T) obtained for the unimolecular dissociation reactions are: $Fe(CO)_5^{\bullet+} \rightarrow Fe(CO)_4^{\bullet+}$ (T = 20 meV), $Fe(CO)_4^{\bullet+} \rightarrow Fe(CO)_3^{\bullet+}$ (T = 12 meV) and $Fe(CO)_3^{\bullet+} \rightarrow Fe(CO)_2^{\bullet+}$ (T = 11 meV). These values correspond to maximum scattering angles of 0.040°, 0.034°, and 0.035°, respectively.[48] Even if the extreme width of the daughter ion peak is considered (T_{max} = 140, 85, and 55 meV), the angles are all less than 0.1° for the neutral particle, CO, and much less for the heavier ionic fragment, $Fe(CO)_n^{\bullet+}$. The corresponding kinetic energy releases under CID conditions are larger, but the correction remains negligible.

$Fe(CO)_5$, $W(CO)_6$, Ar, and He were obtained commercially and used without purification. Perfluoro-2,4-dimethyl-3-ethylpentane (C_9F_{20}) was synthesized at the Instituto Guido Donegani, Novara, Italy.

Results and Discussion

Angle-Resolved CID Spectra of $Fe(CO)_5^{\bullet+}$. Collision-induced dissociation (CID) spectra are shown in Figure 1 for $Fe(CO)_5^{\bullet+}$ ions (m/z 196) accelerated to 3 keV prior to collision upon Ar,

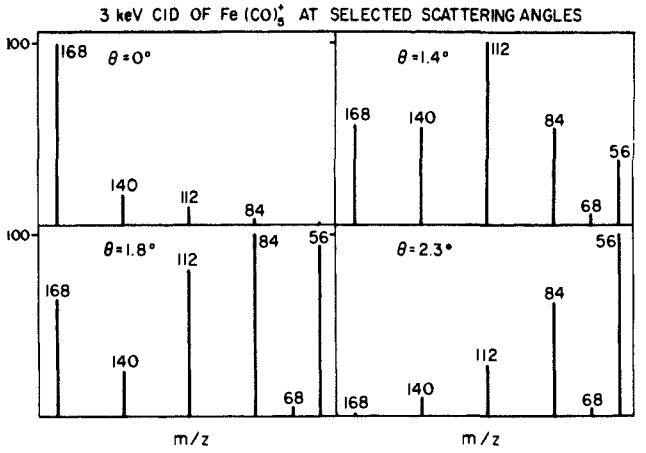

Figure 1. Fragment ion spectra recorded for $Fe(CO)_5^{\bullet+}$ upon collisional activation with Ar at 3 keV for instrument scattering angles of (a) 0°, (b) 1.4°, (c) 1.8°, and (d) 2.3°. The corresponding center-of-mass scattering angles are 0°, 8.3°, 10.7° and 13.6°, respectively.

with product ions collected at scattering angles increasing from 0 to 2.3°. At 0° scattering angle[40] (Figure 1a), loss of a single CO from the parent ion to give $Fe(CO)_4^{\bullet+}$ (m/z 168) is the favored fragmentation process and gives rise to the base peak in the daughter spectrum. Subsequent CO losses occur to increasingly small extents. Since these consecutive fragmentation reactions require that increasing amounts of internal energy be deposited into the ion,[35] it may be concluded that at 3-keV collision energy there is a low probability of depositing a large amount of energy into $Fe(CO)_5^{\bullet+}$ when products are collected at near 0° scattering angle.

CID daughter ion spectra recorded through increasing scattering angles (Figure 1, b–d) display dramatic changes in relative fragment ion abundances.[49] The lower mass fragment ions, which originate through consecutive decarbonylations and require successively larger internal energies for their formation, appear with sharply increased abundances at higher scattering angles. For example, at 1.4° (Figure 1b), $Fe(CO)_2^{\bullet+}$ (m/z 112) is the most abundant fragment species, although all ions from $Fe(CO)_4^{\bullet+}$ (activation energy, E_0 = 1.1 eV)[50] to $Fe^{\bullet+}$ (E_0 = 7.5 eV) are present in significant amounts. At the largest scattering angle, 2.3° (Figure 1d), the $Fe^{\bullet+}$ and $FeCO^{\bullet+}$ ions are principally observed, while higher mass fragments which require less internal energy have decreased abundances, and the lowest activation process is almost completely absent. The large abundances of the $FeCO^{\bullet+}$ and $Fe^{\bullet+}$ ions, which require a minimum of 5.5 and 7.5 eV, respectively, to be produced from the parent ion, confirm previous ARMS results that also noted increasing amounts of internal energy were deposited into the colliding ion at increasing scattering angles.[4,7,8,15] Note that the ion $FeC^{\bullet+}$ (E_0 = 15.6 eV), which arises through a competitive reaction sequence to the main decarbonylation pathway, occurs at the higher scattering angles, although in very low abundance.

Internal Energy Distributions for Scattered $Fe(CO)_5^{\bullet+}$ Ions of 3 keV. $P(\epsilon)$ distributions[54] were approximated from known activation energies for successive decarbonylation reactions,[50] together with recorded fragment ion abundances, using a method previously described.[35] $Fe(CO)_5^{\bullet+}$ and $W(CO)_6^{\bullet+}$ were selected

(43) Jennings, K. R.; Mason, R. S. In *Tandem Mass Spectrometry*; McLafferty, F. W., Ed.; Wiley: New York, 1983; p 197.

(44) Nominal 1×10^{-5} Torr (estimated 1×10^{-4} Torr) corresponds to less than 10% attenuation of the beam and hence to single collision conditions in conventional high-energy CID.

(45) Beynon, J. H.; Cooks, R. G.; Amy, J. W.; Baitinger, W. E.; Ridley, T. Y. *Anal. Chem.* **1973**, *45*, 1023A.

(46) $Fe(CO)_5^{\bullet+}$ ions were generated by charge exchange with $Ar^{\bullet+}$ in a CI ion source. Kinetic energy release measurements were made by scanning the electrostatic analyzer over the fragment ion region of interest. The background pressure was typically 2×10^{-7} Torr inside the analyzer region.

(47) Cooks, R. G.; Beynon, J. H.; Caprioli, R. M.; Lester, G. R. In *Metastable Ions*; Elsevier: Amsterdam, 1973.

(48) Scattering due to kinetic energy release: $\theta_{max} = [(M - m)T/mE_0]^{1/2}$, where M = mass of parent ion, m = mass of fragment ion, T = kinetic energy release for fragmentation, and E_0 = ion kinetic energy (from ref 16).

(49) In addition, the absolute daughter ion abundance decreases with scattering angle, changing by a factor of approximately 50 as the scattering angle is raised from 0° to 2°.

(50) The appearance energies for fragmentation of $Fe(CO)_5^{\bullet+}$ are average values based on ref 51–53.

(51) Junk, G. A.; Svec, J. H. *Z. Naturforsch., Teil B* **1968**, *21*, 1.

(52) Bidinosti, D. R.; McIntyre, M. S. *Can. J. Chem.* **1967**, *45*, 641.

(53) Foffani, A.; Pignataros, *Z. Phys. Chem.* **1965**, *45*, 79.

(54) (a) Kim, M. S.; McLafferty, F. W. *J. Am. Chem. Soc.* **1978**, *100*, 3279. (b) Rabrenovic, M.; Beynon, J. H.; Lee, S. H.; Kim, M. S. *Int. J. Mass Spectrom. Ion Processes* **1985**, *65*, 197. (c) McLafferty, F. W.; Bente, P. F., III; Kornfeld, R.; Tsai, S.-C.; Howe, I. *J. Am. Chem. Soc.* **1973**, *95*, 2120. (d) Vekey, K.; Brenton, A. G.; Beynon, J. H. *J. Phys. Chem.* **1986**, *90*, 3569.

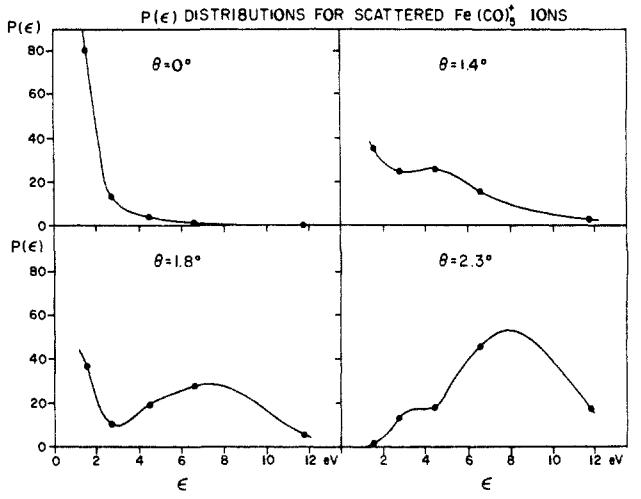

Figure 2. Internal energy distributions for $Fe(CO)_5^{\bullet+}$ upon 3-keV collisional activation with Ar, determined using the data in Figure 1.

for this study since they allow $P(\epsilon)$ to be estimated using several simplifying assumptions: (i) the ions fragment by a series of consecutive reactions, all having known activation energies; (ii) the entropy requirements for each fragmentation are similar; and (iii) there are negligible kinetic effects; i.e., all ions with sufficient internal energy dissociate via the most endothermic reaction pathway available. The method of approximating $P(\epsilon)$ distributions is illustrated for the reaction sequence:

$$Fe(CO)_5^{\bullet+} \rightarrow Fe(CO)_4^{\bullet+} \rightarrow Fe(CO)_3^{\bullet+} \rightarrow Fe(CO)_2^{\bullet+} \rightarrow FeCO^{\bullet+} \rightarrow Fe^{\bullet+}$$

All parent ions with internal energies between the activation energies $[E_0(1)]$ and $[E_0(2)]$, required for formation of the fragment ions $Fe(CO)_4^{\bullet+}$ and $Fe(CO)_3^{\bullet+}$, respectively, are assumed to fragment to yield the $Fe(CO)_4^{\bullet+}$ ion. Parent ions with internal energies between $[E_0(2)]$ and $[E_0(3)]$ fragment to give $Fe(CO)_3^{\bullet+}$, and so on for the lower mass fragments. The relative abundance of the various fragment ions in the daughter ion spectrum represents the fraction of parent ions with internal energies which fall in a particular internal energy interval. The abundance of the $Fe(CO)_4^{\bullet+}$ ion, divided by the energy range $E_0(2) - E_0(1)$, gives the magnitude of the point in the distribution $P(\epsilon)$ at an energy $\epsilon = [E_0(1) + E_0(2)]/2$. The $P(\epsilon)$ distribution is mapped by following this procedure for each of the observed fragments.

Internal energy distributions, illustrated in Figure 2, were determined from the ARMS daughter ion spectra (Figure 1), using the method just described. The distribution at 0° scattering angle (Figure 2a) has a low-probability, high-energy tail, as expected for high-energy collisional activation.[35,54,55] The curves obtained for scattered ions (Figure 2, b–d) establish that increasing average internal energies, $\bar{\epsilon}$, are deposited during CID as the scattering angle is increased. For example, as θ is raised from 0° to 2.3° (Figure 2d), $\bar{\epsilon}$ increases from ca. 1 eV to more than 8 eV. Moreover, $\bar{\epsilon}$ can be continuously shifted across the entire energy range, simply by selecting the appropriate observation angle. A remarkable feature of the $P(\epsilon)$ data is their structured nature, particularly at intermediate scattering angles (Figure 2c), where the internal energy distribution displays a bimodal shape, one peak lying centered at low energy (ca. <3 eV) and the second shifting toward higher energies as the scattering angle is increased.

Internal Energy Distributions in Other Experiments. The effect of collision energy, E, on the $P(\epsilon)$ distributions in ARMS was investigated by recording daughter ion spectra of $Fe(CO)_5^{\bullet+}$ at 1.5- and 2-keV collision energies. In Figure 3, $P(\epsilon)$ curves are displayed for $Fe(CO)_5^{\bullet+}$ activated through 1.5-keV collisions upon Ar at scattering angles which increase from 0 to 2.3°. As in the $P(\epsilon)$ distributions obtained at 3 keV, the average internal energy, $\bar{\epsilon}$, increases rapidly as the scattering angle is raised, and a direct comparison between the 1.5- and 3-keV data indicates that, for

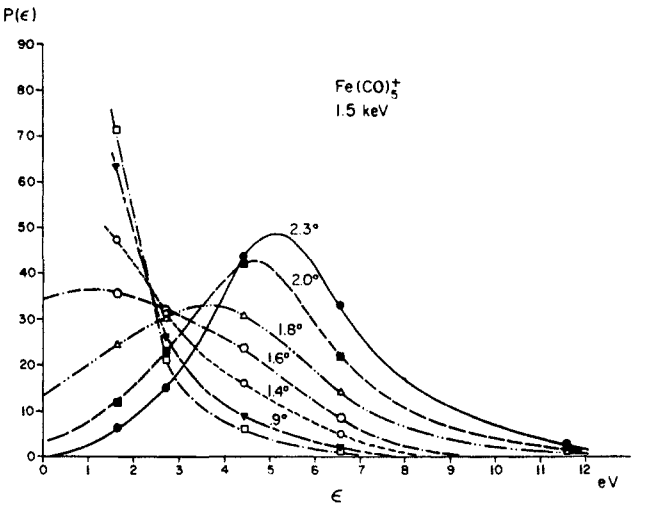

Figure 3. Internal energy distributions determined for $Fe(CO)_5^{\bullet+}$ at increasing scattering angles following collisional activation upon Ar at 1.5 keV. Lab angles are 0 to 2.3°.

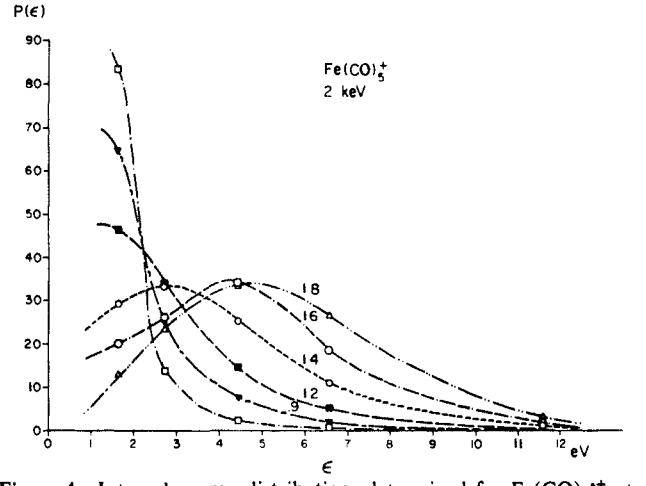

Figure 4. Internal energy distributions determined for $Fe(CO)_5^{\bullet+}$ at increasing scattering angles following collisional activation upon Ar at 2 keV. Lab angles are 0 to 1.8°.

all values of θ, larger amounts of internal energy are deposited at the higher collision energy. A noteworthy feature of all the 1.5-keV distributions is that they have approximately Gaussian shapes, whose maximum shifts from 1 to 5 eV as the scattering angle is increased from 0 to 2.3°. These curves do not display bimodal shapes, as observed for the $P(\epsilon)$ distributions obtained at 3 keV.

Because of the differences in the shapes of the $P(\epsilon)$ distributions at 1.5 and 3 keV, daughter ion spectra were also acquired at 2-keV collision energy. Scattering angles ranging from 0 to 1.8° were recorded and Ar again was used as the target for collisional activation. The resulting $P(\epsilon)$ curves, illustrated in Figure 4, resemble the distributions obtained at 1.5 keV, although there is an indication of the bimodal shape observed in the 3-keV collisions at the larger scattering angles. The maxima (ϵ_{max}) and average ($\bar{\epsilon}$) internal energies are shifted toward higher values relative to the 1.5-keV data. For example, an average internal energy of 5 eV is found at a scattering angle of ca. 1.8° at 2 keV, while in the 1.5-keV experiment, scattering through 2.3° is necessary to observe ions with the same average energy. To a good approximation, the 2-keV distributions lie between the 1.5- and 3-keV curves. All data obtained at 1.5 and 2 keV support the results obtained at the higher collision energy; that is, the average internal energy deposited during the collision increases as the value of E or θ is increased.

Internal energy distributions were also determined for $W(CO)_6^{\bullet+}$ ions which underwent scattering in the course of activation. The activation energies for decarbonylation reactions

Table I. Internal Energy Distributions Determined for $W(CO)_6^{\bullet+}$ Activated by Collision with He, Ar, and C_9F_{20} (MW 488) at 3.0 keV with Product Collection at the Indicated Laboratory Scattering Angles

	He, %			Ar, %			C_9F_{20}, %		
$P(\epsilon)$, eV	0°	1.2°	2.0°	0°	1.2°	2.0°	0°	1.2°	2.0°
2.3	74.0	54.0	68.4	70.0	43.6	28.4	76.7	42.0	41.1
4.3	19.0	31.5	23.0	17.8	29.5	18.6	14.6	31.0	18.5
6.35	5.1	10.9	6.5	8.5	17.1	25.9	6.7	16.1	17.1
8.8	1.5	2.8	2.1	2.8	6.9	17.9	1.4	6.0	11.0
11.55	0.4	0.8		0.8	2.5	7.5	0.6	3.4	7.6
15.2				0.1	0.4	1.7		1.5	4.7

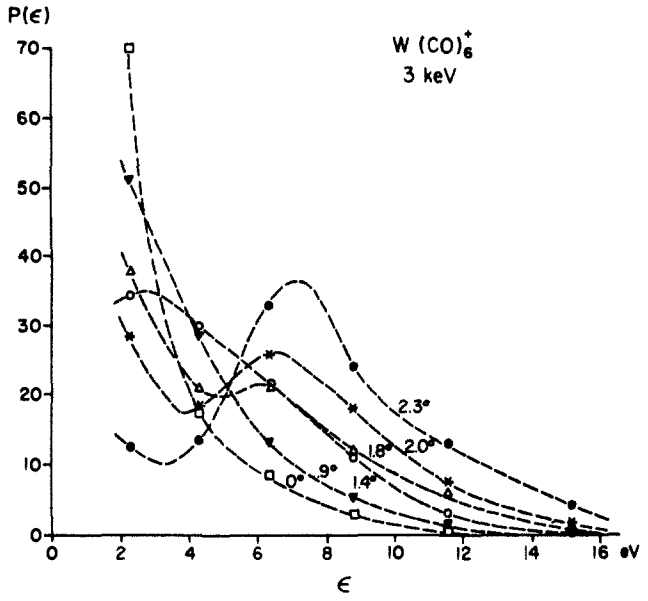

Figure 5. Internal energy distributions determined for $W(CO)_6^{\bullet+}$ at increasing scattering angles following collisional activation upon Ar at 3 keV. Lab angles are 0 to 2.3°.

in $W(CO)_6^{\bullet+}$ are higher than those for $Fe(CO)_5^{\bullet+}$ (i.e., for $Fe(CO)_5^{\bullet+}$, $E_0(1) = 1.1$ eV, $E_0(2) = 2.1$ eV, $E_0(3) = 3.3$ eV, $E_0(4) = 5.5$ eV, and $E_0(5) = 7.5$ eV, where $E_0(n)$ is the activation energy for loss of (n) molecules of CO;[50,55] while for $W(CO)_6^{\bullet+}$, $E_0(1) = 1.2$ eV, $E_0(2) = 3.4$ eV, $E_0(3) = 5.2$ eV, $E_0(4) = 7.5$ eV, $E_0(5) = 10.1$ eV, and $E_0(6) = 13.0$ eV[57,58]). This makes definition of the shape of $P(\epsilon)$ in zero-angle scattering experiments a little more difficult than is the case for $Fe(CO)_5^{\bullet+}$. With $W(CO)_6^{\bullet+}$ though, higher internal energies can be recorded, and this system therefore complements the data obtained using $Fe(CO)_5^{\bullet+}$.

In Figure 5, $P(\epsilon)$ distributions are shown for $W(CO)_6^{\bullet+}$ ions collected through scattering angles up to 2.3° following 3-keV collision upon Ar. Many of the features associated with the $P(\epsilon)$ distributions for $Fe(CO)_5^{\bullet+}$ are repeated for $W(CO)_6^{\bullet+}$. The average internal energy, $\bar{\epsilon}$, increases with the scattering angle, and rather large internal energies (>15 eV for $W(CO)_6^{\bullet+}$) are deposited with quite high probability at large scattering angles. Of particular interest are the bimodal distributions observed for $W(CO)_6^{\bullet+}$ at scattering angles greater than 1.6°. $P(\epsilon)$ distributions were also determined at 1.5 keV for $W(CO)_6^{\bullet+}$ (supplementary material), and they closely resemble the distributions found for $Fe(CO)_5^{\bullet+}$ at the lower collision energy. Their shapes are nearly Gaussian and the average internal energy deposited upon collision increases as the scattering angle is raised.

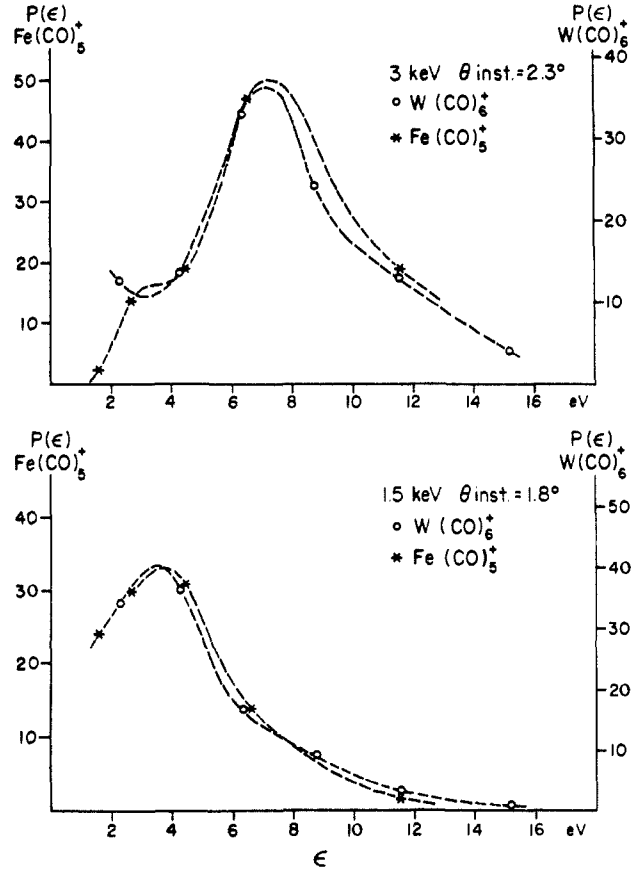

Figure 6. Comparison of internal energy distributions for collisionally activated $Fe(CO)_5^{\bullet+}$ and $W(CO)_6^{\bullet+}$ ions following (a, top) 3-keV collision upon Ar at 2.3° laboratory scattering angle and (b, bottom) 1.5 keV with products collected at 1.8°.

$P(\epsilon)$ distributions for $Fe(CO)_5^{\bullet+}$ and $W(CO)_6^{\bullet+}$ at identical *laboratory*-scattering angles and collision energies are very similar, despite the large differences in the *center-of-mass* collision energies (E_{cm}) and scattering angles (θ_{cm}) for these two systems.[59] In small-laboratory scattering-angle experiments ($\theta < 1.2°$), slightly larger internal energies are deposited into $W(CO)_6^{\bullet+}$ than $Fe(CO)_5^{\bullet+}$ upon collision with Ar at a given scattering angle and collision energy. As the scattering angle is raised, the distributions become very similar (Figure 6). At 3-keV collision energy and 2.3° scattering angle the two $P(\epsilon)$ curves are nearly identical, even though there are large differences in the center-of-mass parameters, viz., $Fe(CO)_5^{\bullet+}$, $E_{cm} = 508$ eV and $\theta_{cm} = 13.5°$ for a 3-keV collision upon Ar, while for $W(CO)_6^{\bullet+}$, under the same laboratory conditions, $E_{cm} = 306$ eV and $\theta_{cm} = 23°$. The high degree of similarity can be attributed to the nearly identical reduced collision parameters $(E\theta)_{cm}$ associated with these two systems, i.e., for $Fe(CO)_5^{\bullet+}$ upon Ar, $(E\theta)_{cm} = 6858$ eV deg, and for $W(CO)_6^{\bullet+}$, $(E\theta)_{cm} = 7038$ eV deg. Likewise, at 1.5 keV and 1.8° laboratory scattering angle, the $P(\epsilon)$ distributions are nearly the same; in this case $E_{cm} = 254$ eV and $\theta_{cm} = 10.8°$ ($(E\theta)_{cm} = 2743$ eV deg) for

(55) The maximum internal energy deposited is about 7 eV. Formation of FeC^+ (activation energy, $E_0 = 15.6$ eV) allows a point at 11.6 eV on the internal energy distribution to be interrogated (ref 56).

(56) This rearrangement ion does not satisfy the kinetic criteria desired to establish $P(\epsilon)$ distributions, and hence this point in the distribution is somewhat uncertain.

(57) The appearance energies for fragmentation of $W(CO)_6^{\bullet+}$ are average values based on ref 51–53.

(58) The rearrangement ion $WC^{\bullet+}$ activation energy (E_0) is 20.3 eV, and use of this ion allows a point at ca. 15 eV on the internal energy distribution to be interrogated (see also ref 56).

(59) McDaniel, E. W. In *Collision Phenomena In Ionized Gases*; Wiley: New York, 1964.

$Fe(CO)_5^{\bullet+}$ upon Ar, while for $W(CO)_6^{\bullet+}$, E_{cm} = 153 eV and θ_{cm} = 18° ($(E\theta)_{cm}$ = 2754 eV deg).

To learn more about the collision mechanism, the role of the target gas in internal energy deposition at nonzero scattering angles was examined.[5,6,18] Helium and perfluoro-2,4-dimethyl-3-ethylpentane (C_9F_{20}) (m/z 488) were selected as additional target gases. $P(\epsilon)$ distributions for collisional activation of $W(CO)_6^{\bullet+}$ upon He, Ar, and C_9F_{20} at 3 keV are given in Table I at 0°, 1.2°, and 2.0° scattering angles.

In the zero-angle experiment the three targets give similar results, Ar depositing slightly more internal energy than either He or C_9F_{20}. (Note that the common choice of He for CID experiments is made on the basis of its small probability of causing neutralization or scattering out of the acceptance cone of the mass spectrometer.[5-7]) At 1.2° scattering angle, substantial differences were observed for the three targets. He, compared to Ar and C_9F_{20}, deposits a smaller average internal energy, although more energy is deposited at the small nonzero scattering angle than at 0°. The center-of-mass collision energy and scattering angle for collision of $W(CO)_6^{\bullet+}$ upon He at 3 keV and 1.2° scattering angle differ considerably from those associated with collision upon Ar. The relatively small E_{cm} available using He (E_{cm} = 33 eV) may limit the amount of internal energy which can be transferred to the $W(CO)_6^{\bullet+}$ ion. On the other hand, C_9F_{20} behaves much like Ar at 1.2° scattering angle, except that with the heavier target slightly larger internal energies are deposited. At 2.0° scattering angle, C_9F_{20} again produces nearly the same degree of fragmentation as that found with Ar, even though a considerably higher center-of-mass collision energy is available for the heavier target (E_{cm} = 1750 eV vs 306 eV for Ar). Clearly this polyatomic target is not behaving like a single entity,[32,60] and this is consistent with vibrational excitation in an impulsive collision in which some atoms of the target act as spectators during the collision. An additional consideration is that collisions with a polyatomic target may lead to target excitation or target ionization.[61]

At 2.0° scattering angle, the internal energy deposited upon collisions with helium decreases relative to 1.2° (Table I). In sharp contrast to Ar and C_9F_{20}, collision upon He results in an internal energy deposited which goes through a maximum as the scattering angle is increased. Apparently He is unable to scatter massive ions such as $W(CO)_6^{\bullet+}$ through large scattering angles in one step of collisional activation at kiloelectron volt energies.[5,7] Note that for collision of $W(CO)_6^{\bullet+}$ upon He, θ_{cm} reaches 90° at a laboratory scattering angle of 0.65°, whereas with Ar, at θ_{cm} = 90° the laboratory angle is 6.5°. This suggests that He may use two or more collisions to produce 2° laboratory scattering. Possibly the markedly different behavior noted for He versus the other targets can be attributed to multiple collisions at nonzero scattering. Since the internal energy transferred upon each scattering collision would be small, multiple collision conditions might lead to the observed smaller degree of excitation observed at the largest angles. Peculiarities in the behavior of He as a target gas have also been noted by others,[18] who suggested that these collisions involve particularly short-range interactions due to the tightness with which the two He electrons are bound to the nucleus. Highly efficient nuclear screening results in inefficient excitation at nonzero scattering angles, as indicated by the rapid falloff in cross sections for excitation with increasing scattering angle.

Further Discussion on the ARMS Experiment and the Method for Estimating Internal Energy Distributions. The $P(\epsilon)$ distributions reflect the amount of internal energy deposited into the selected ion upon collisional activation. There are several factors which may affect the accuracy of these curves, and they are considered in turn. Inaccurate recording of ion intensities and contributions from the precollision internal energy of the ion[35,62] are minor inaccuracies and can be ignored. The extreme high internal energy region of the $P(\epsilon)$ curves is not well defined,[33,55] especially for $Fe(CO)_5^{\bullet+}$, since it is determined by utilizing nonconsecutive fragmentation processes (i.e., $FeCO^{\bullet+}$ formed by direct bond cleavage versus $FeC^{\bullet+}$ formed by rearrangement) with large differences in activation energies (E_0 = 7.5 and 15.6 eV, respectively[50]), and possibly different reaction kinetics. Competitive reactions other than the formation of $FeC^{\bullet+}$ are not observed for CID of $Fe(CO)_5^{\bullet+}$. On the other hand, $W(CO)_6^{\bullet+}$ undergoes substantial rearrangement (up to 5% of the recorded signal at the larger scattering angles), leading to the formation of a series of ions $WC(CO)_x^{\bullet+}$ (x = 1–4). These rearrangement ions increase in abundance as the scattering angle and collision energy are raised and occur more readily upon activation with the heaviest target, C_9F_{20}.

The range of scattering angles recorded in the ARMS experiment will strongly influence the shapes of the $P(\epsilon)$ distributions. With the SIMION ion optical program,[42] an ion beam with a height of 5 mm in the nonfocusing xz direction is shown to encompass a range of angles of up to ±0.25° at 2.3° scattering angle, leading to poor angular resolution along the axis of deflection. The range of angles sampled in the focusing xy plane is determined by the entrance and β-slit widths, as well as the range of ion kinetic energies which are sampled using the B/E-linked scan.[43] Even though a range of angles which is not well defined is sampled in these experiments, the principal consequence will be to reduce the resolution of features in the $P(\epsilon)$ distributions, and this may account for the difficulty in observing the bimodal structure in the 2-keV data. The match with data obtained previously in an instrument where slits were used to collect highly a collimated beam of ions[7,15] confirms that the angles selected in these experiments are not grossly in error.

As mentioned earlier, release of kinetic energy during dissociation may contribute to ion scattering.[4,15-19,22] Decarbonylation reactions in the metal carbonyl ions, however, have small kinetic energy releases, and only a small fraction of the total scattering can be attributed to the release of kinetic energy (see Experimental Section). Moreover, ARMS experiments performed in the absence of collision gas yield only the $(M - CO)^{\bullet+}$ ion, and this is present in very low abundance. It may be inferred that scattering observed in these ARMS experiments is due mainly to the collision process and not to metastable ion dissociations.

A related issue already alluded to is the possible occurrence of multiple collisions. The ARMS experiments were conducted in such a manner that multiple collision conditions for zero-angle scattering should have been accessible, but even at high-collision gas pressures, which resulted in a parent ion beam attenuation of more than 60%,[63] significant changes in fragment ion ratios were not observed. This is attributed to the occurrence of competitive processes of larger cross section (elastic scattering and charge exchange[6,7]) which keep CID in the single collision regime. The cross sections for scattering ions through increasing angles in keV collisions decreases rapidly.[1,3,24,25] As the scattering angle increases, the cross section drops and the pressure required to access multiple-collision conditions rises proportionately (Beer's law). It is therefore probable that sufficiently high pressures for more than a single nonzero-angle collision were not reached, except perhaps for experiments with the He target. This accounts for the lack of pressure effects on the data, except with He. For collisions upon He, it may have been possible to access multiple collision conditions at the nominal pressure of 1×10^{-5} Torr used, although it is extremely difficult to determine the actual target pressure within the collision cell.

Mechanism of Ion Activation in High-Energy CID. Notable features of the $P(\epsilon)$ distributions for $Fe(CO)_5^{\bullet+}$ and $W(CO)_6^{\bullet+}$ are their structured nature and the strong dependence of the structure on the collision parameters (E and θ). By comparing

(60) Kessel, Q. C.; Pollack, E.; Smith, W. W. In *Collision Spectroscopy*; Cooks, R. G., Ed.; Plenum Press: New York, 1978; Chapter 3.

(61) (a) Bricker, D. L.; Russell, D. H. *J. Am. Chem. Soc.* **1986**, *108*, 6174. (b) The degree of target excitation cannot be measured by methods available to us. Translational endothermicity measurements are not sufficiently accurate, especially when one considers the large elastic energy loss associated with nonzero scattering.

(62) The maximum internal energy prior to collision is assumed to be equal to the activation energy of the lowest energy fragmentation. For $Fe(CO)_5^{\bullet+}$ the maximum initial internal energy is less than 1.1 eV.

(63) Holmes, J. L. *Org. Mass Spectrom.* **1985**, *20*, 169.

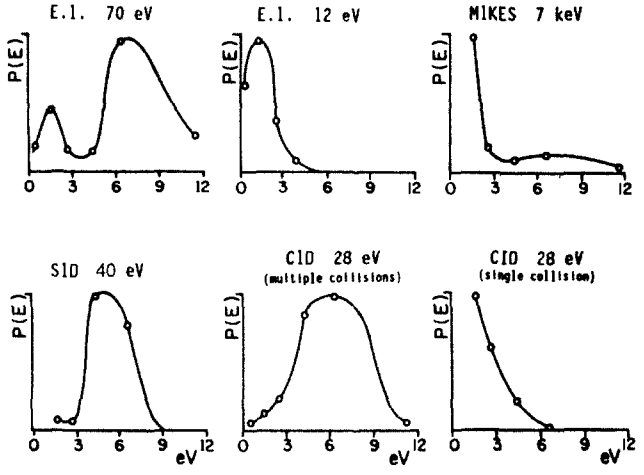

Figure 7. Internal energy distributions for $Fe(CO)_5^{\bullet+}$ activated by several methods: (a) 70-eV EI, (b) 12-eV EI, (c) 7-keV CID, (d) 40-eV SID, (e) 28-eV CID multiple collisions, (f) 28-eV CID single collision. Argon was used as the collision gas in all CID experiments.

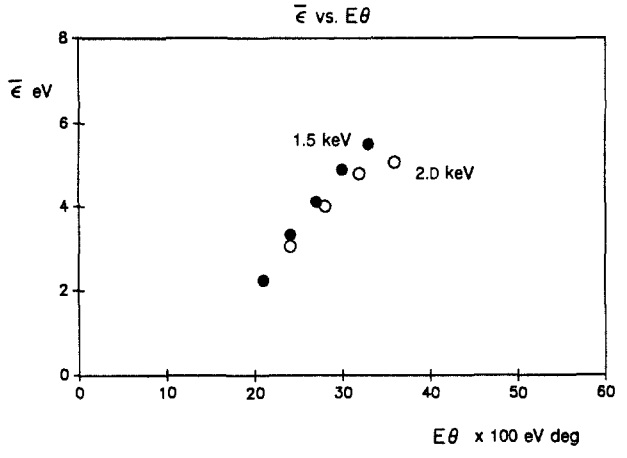

Figure 8. Plot of average $Fe(CO)_5^{\bullet+}$ internal energy ($\bar{\epsilon}$) versus the reduced scattering parameter $E\theta$ for experiments covering collision energies (E) ranging from 1.5 to 2.0 keV and scattering angles (θ) from 1 to 2.3°.

$P(\epsilon)$ distributions obtained for scattered $Fe(CO)_5^{\bullet+}$ ions with those found using other activation methods (Figure 7), including electron impact (EI), low-energy CID,[64] and surface-induced dissociation (SID),[65] interpretation of the information on the transfer of translational to internal energy in kiloelectron volt collisions is facilitated. In electron impact (Figure 7, a and b), where direct electronic excitation occurs and strict Franck–Condon factors govern the formation and internal energy of the ionic species,[66] the region in the $P(\epsilon)$ distribution between 3 and 5 eV is not populated. The presence of gaps in the accessible excited states of the ion during this purely electronic excitation mode is also evident in the photoelectron spectrum.[67] At zero-scattering angle in the CID experiment, Figures 2a and 7c, the $P(\epsilon)$ distribution has a maximum internal energy below 3 eV, and the region above 3 eV is not highly populated. By way of contrast, in the nonzero angle CID experiments (Figure 2, b–d), the region between 3 and 5 eV in the $P(\epsilon)$ distribution is readily populated, and a strong dependence upon the parameters E and θ is observed. $W(CO)_6^{\bullet+}$ displays highly similar behavior. The region between 2 and 4 eV in the $P(\epsilon)$ distribution, which is unpopulated upon EI excitation,[35] is strongly populated at nonzero scattering angles. These results suggest the occurrence of a combination of excitation mechanisms, vibrational excitation in addition to electronic excitation.

Further evidence for participation of vibrational excitation in kiloelectron volt collisions comes from data for excitation of $Fe(CO)_5^{\bullet+}$ at a solid surface.[65] In this low-energy, large-angle, vibrational excitation experiment,[68] a narrow distribution of internal energies is deposited, and this energy may be shifted across the internal energy scale by simply varying the collision energy. Figure 7d shows that the region from 3 to 5 eV in the SID $P(\epsilon)$ distribution is readily populated. These features match closely the 1.5- and 2-keV $P(\epsilon)$ distributions for nonzero angle CID (Figures 3 and 4), where the maximum can be continuously shifted toward higher ϵ values by raising the scattering angle. It is of interest to note that the reduced scattering parameter ($E\theta$)[59,69] which describes atomic collision phenomena is very similar in these two otherwise very different experiments. Thus $E\theta$ = 1500 eV × 2° = 3000 eV deg for the CID experiment at 1.5 keV and 2° scattering angle (Figure 3), and $E\theta$ = 40 eV × 90° = 3600 eV deg for the SID experiment shown in Figure 7d. Although the nature of the target will affect energy deposition also, the agreement between the $P(\epsilon)$ distributions for these experiments is strong evidence that the high-energy CID process occurs by vibrational excitation. Figure 7, e and f, shows the energy distributions which result from low-energy CID, a process known to occur by vibrational excitation. The maximum energy (6 eV) deposited in a single collision (28 eV) matches the sum of the center-of-mass collision energy (4.7 eV) and the maximum internal energy which the metastable ions can carry (estimated to be slightly larger than the activation energy for the lowest energy dissociation process, which is 1.1 eV).

Additional support for the proposal that vibrational excitation occurs in the small-angle, keV energy collisions is found in the plot of the collision parameter ($E\theta$) versus the average internal energy ($\bar{\epsilon}$) deposited during the collision. To a good approximation the average energy $\bar{\epsilon}$ of the activated ion is equal to $\Delta\epsilon$, since the initial internal energy is small (less than the smallest activation energy[62]). The $\bar{\epsilon}$ versus $E\theta$ plot is shown in Figure 8.[70] Earlier work[12] on vibrational excitation at *low* collision energies established a linear relationship between the internal energy deposited in the projectile ($\Delta\epsilon$), and the scattering angle (θ) and collision energy (E), in the form $\Delta\epsilon \propto E\theta$. In earlier work in the keV range, dependencies on both the collision energy and the scattering angle have been demonstrated,[5-7] although the form of the dependencies has not been secured, in spite of considerable effect.[17-19,22] Although a broad range of scattering angles are sampled in our experiment, our data show that $\bar{\epsilon}$ increases approximately linearly with θ. The dependence of our data on θ^2 is nonlinear; however, the data are not sufficiently precise to exclude power dependencies other than $\Delta\epsilon \propto E\theta$.

We must emphasize that the evidence that vibrational excitation plays a major role in kiloelectron volt collisions, resulting in laboratory scattering angles of few degrees, does not imply that electronic excitation is absent. In 3-keV collisions, where the products are collected through nonzero scattering angles, a bimodal $P(\epsilon)$ distribution is observed. Based on the above arguments it may well be that the first peak, occurring at lower internal energy values, represents electronic excitation, perhaps of the oblique type,[25] where it is accompanied by vibrational excitation, whereas the peak at higher ϵ values corresponds to direct vibrational ex-

(64) (a) Kenttämaa, H. I.; Cooks, R. G. *J. Am. Chem. Soc.* **1985**, *107*, 1881. (b) Dawson, P. H.; Sun, F. W. *Int. J. Mass Spectrom. Ion Processes* **1982**, *33*, 51. (c) McLuckey, S. A.; Ouwerkerk, C. E. D.; Boerboom, A. J. H.; Kistemaker, P. G. *Int. J. Mass Spectrom. Ion Processes* **1984**, *59*, 85.

(65) (a) Dekrey, M. J.; Kenttämma, H. I.; Wysocki, V. H.; Cooks, R. G. *Org. Mass Spectrom.* **1986**, *21*, 193. (b) Bier, M. E.; Amy, J. W.; Cooks, R. G.; Syka, J. E. P.; Ceja, P.; Stafford, G. *Int. J. Mass Spectrom. Ion Processes* **1987**, *77*, 31.

(66) Hasted, J. B. In *Physics of Atomic Collisions*; Butterworths: London, 1964.

(67) (a) Turner, D. W.; Baker, C.; Baker, A. D.; Brundle, C. R. In *Molecular Photoelectron Spectroscopy*; Interscience: New York, 1969. (b) Eberhardt, W.; Plummer, E. W.; Chen, C. T.; Ford, W. K. *Aust. J. Phys.* **1986**, *39*, 853.

(68) Cooks, R. G.; Mabud, Md. A.; Horning, S. R.; Jiang, X.-Y.; Paradisi, C.; Traldi, P. *J. Am. Chem. Soc.* **1989**, *111*, 859.

(69) Johnson, R. E.; Boring, J. W. In *Collision Spectroscopy*; Cooks, R. G., Ed.; Plenum Press: New York, 1978; Chapter 2.

(70) The data for 3-keV collisions is not included because of the presence of the second component in the internal energy distributions. In addition, data taken at the smallest angles give uncertain average energies and are excluded.

citation. This is further supported by the observation that the position of the lower energy peak coincides approximately with that observed in the electron impact $P(\epsilon)$ distribution (Figure 7a,b). In the 1.5- and 2-keV collision energy experiments, the $P(\epsilon)$ distributions no longer display structured profiles. This is probably due to the increased contribution of vibrational excitation at lower collision energies. Thus, activation of the parent ion by means of a vibrational mechanism is favored (i) by increasing the scattering angle and (ii) by decreasing the ion collision energy. A complete interpretation of the shapes of the $P(\epsilon)$ distributions remains difficult though. For example, at higher collision energies (7 keV) the zero-angle CAD experiment begins to show a bimodal structure (Fugre 7c), perhaps because the zero-angle experiment includes off-axis contributions which, in combination with the large value of E, give $E\theta$ a significant value.

Conclusion

The internal energy deposited in $Fe(CO)_5^{\bullet+}$ and $W(CO)_6^{\bullet+}$ ions increases as the scattering angle at which products are collected is raised. The average energy transferred also varies with collision energy, increasing monotonically with the scattering parameter, $E\theta$. The internal energy distributions associated with these kiloelectron volt energy collision processes show structure at larger values of $E\theta$. This structure is compared with that seen in electron impact and with the unstructured curves observed in low-energy ion/surface and gaseous collisions. These comparisons suggest that the major contribution to collision-induced dissociation in ARMS experiments in the keV energy range is made by vibrational excitation. The smaller, lower energy deposition component observed under some conditions is apparently due to simple electronic excitation. This latter conclusion must be recognized as tentative only; a significant alternative is that oblique collisions contribute to collisional activation. Much more needs to be learned about collisional dynamics before the second mechanism can be evaluated in more detail.

Acknowledgment. This work was supported by the National Science Foundation (CHE 87-21768).

Registry No. He, 7440-59-7; Ar, 7440-37-1; C_9F_{20}, 50285-18-2; $Fe(CO)_5^+$, 59699-78-4; $W(CO)_6^+$, 112908-02-8.

Supplementary Material Available: Figures showing internal energy distributions for $Fe(CO)_5^{\bullet+}$ at 3.0 keV and $W(CO)_6^{\bullet+}$ at 1.5 keV and tables of normalized daughter spectra (9 pages). Ordering information is given on any current masthead page.

Photoinduced Charge Separation in a Porphyrin–Tetraviologen Supramolecular Array

James D. Batteas,[†] Anthony Harriman,*[,†] Yu Kanda,[‡] Noboru Mataga,*[,‡] and Andreas K. Nowak[§]

Contribution from the Center for Fast Kinetics Research, University of Texas at Austin, Austin, Texas 78712, Department of Chemistry, Faculty of Engineering Science, Osaka University, Toyonaka, 560 Osaka, Japan, and Davy Faraday Research Laboratory, The Royal Institution, 21 Albemarle Street, London W1X 4BS, U.K. *Received March 3, 1989*

Abstract: A porphyrin–tetraviologen supramolecule P–V_4, in which a viologen molecule is appended to each of the porphyrin meso positions via a 1,3-propanoxy-4-phenyl chain, has been studied by picosecond and nanosecond laser flash photolysis techniques. In DMSO solution, rapid charge separation (CS) occurs from the first excited singlet state of the porphyrin, giving rise to long-lived redox products. These products recombine via first-order kinetics ($\tau = 6.4 \pm 0.7$ μs) to restore the ground-state reactants. Similar, but much slower, CS takes place from the porphyrin triplet excited state, which is formed in competition to CS from the singlet state. Quantum yields for formation of redox products and rates of both CS and charge recombination (CR) are solvent dependent, protic solvents favoring rapid CR.

There is much current interest in the design and study of molecular models capable of mimicking the rapid electron-transfer processes that occur in photosynthetic reaction center complexes.[1] Most models employ a chromophore covalently linked to an electron acceptor or donor via a flexible or rigid spacer group. In many cases, a porphyrin has been used as the chromophore and either a quinone,[2-7] a viologen,[8-12] or a similar electron affinic species[13] functions as electron acceptor.[14] With the use of time-resolved fluorescence spectroscopy and ultrafast flash photolysis techniques, rate constants for charge separation (CS) and charge recombination (CR) have been determined and, in several instances, related to fundamental properties of the system. The effects of solvent, mutual orientation, separation distance, exoergicity, and type of spacer group upon the rates of CS and CR are among the main parameters being investigated at present.[2-14] In closely related studies, the factors affecting intramolecular energy transfer[15] and charge-shift reactions[16] are being monitored.

More elaborate models have been synthesized in which two different electron acceptors have been attached to a single

[†] University of Texas at Austin.
[‡] Osaka University.
[§] The Royal Institution.

(1) (a) Harriman, A. *Energy Resources through Photochemistry and Catalysis* Gratzel, M. Ed.; Academic Press: New York, 1983; p 163. (b) Wasielewski, M. R. *Photochem. Photobiol.* **1988**, *47*, 923. (c) Connolly, J. S.; Bolton, J. R. *Photoinduced Electron Transfer. Part D. Applications*; Fox, M. A. Chanon, M., Eds.; Elsevier: Amsterdam, 1988; p 303. (d) Mataga, N. *Photochemical Energy Conversion*; Norris, J. R., Meisel, D., Eds.; Elsevier: New York, 1989; p 32.

(2) (a) Kong, J. L. Y.; Loach, P. A. *J. Heterocycl. Chem.* **1980**, *17*, 737. (b) Kong, J. L. Y.; Spears, K. G.; Loach, P. A. *Photochem. Photobiol.* **1982**, *35*, 545.

(3) (a) Ho, T.-F.; McIntosh, A. R.; Bolton, J. R. *Nature (London)* **1980**, *254*, 86. (b) Siemiarczuk, A.; McIntosh, A. R.; Ho, T.-F.; Stillman, M. J.; Roach, K. J.; Weedon, A. C.; Bolton, J. R.; Connolly, J. S. *J. Am. Chem. Soc.* **1983**, *105*, 7224. (c) Schmidt, J. A.; McIntosh, A. R.; Weedon, A. C.; Bolton, J. R.; Connolly, J. S.; Hurley, J. K.; Wasielewski, M. R. *J. Am. Chem. Soc.* **1988**, *110*, 1733.

(4) (a) Nishitani, S.; Karata, N.; Sakata, Y.; Misumi, S.; Migita, M.; Okada, T.; Mataga, N. *Tetrahedron Lett.* **1981**, *22*, 2099. (b) Migita, M.; Okada, T.; Mataga, N.; Nishitani, S.; Karata, N.; Sakata, Y.; Misumi, S. *Chem. Phys. Lett.* **1981**, *84*, 263. (c) Mataga, N.; Karen, A.; Okada, T.; Nishitani, S.; Kurata, N.; Sakata, Y.; Misumi, S. *J. Phys. Chem.* **1984**, *88*, 5138.

0002-7863/90/1512-126$02.50/0